Monthly Notices
of the
ROYAL ASTRONOMICAL SOCIETY

Mon. Not. R. Astron. Soc. **410,** 2291–2301 (2011) doi:10.1111/j.1365-2966.2010.17599.x

Galaxy and mass assembly (GAMA): dust obscuration in galaxies and their recent star formation histories

D. B. Wijesinghe,[1⋆] A. M. Hopkins,[2] R. Sharp,[2] M. Gunawardhana,[1] S. Brough,[2] E. M. Sadler,[1] S. Driver,[3] I. Baldry,[4] S. Bamford,[5] J. Liske,[6] J. Loveday,[7] P. Norberg,[8] J. Peacock,[8] C. C. Popescu,[9] R. J. Tuffs,[10] J. Bland-Hawthorn,[1] E. Cameron,[11] S. Croom,[1] C. Frenk,[12] D. Hill,[3] D. H. Jones,[2] E. van Kampen,[6] L. Kelvin,[3] K. Kuijken,[13] B. Madore,[14] B. Nichol,[15] H. Parkinson,[8] K. A. Pimbblet,[16] M. Prescott,[4] A. S. G. Robotham,[3] M. Seibert,[13] E. Simmat,[10] W. Sutherland,[17] E. Taylor[1] and D. Thomas[12]

[1]*Sydney Institute for Astronomy, School of Physics, University of Sydney, NSW 2006, Australia*
[2]*Anglo Australian Observatory, PO Box 296, Epping, NSW 1710, Australia*
[3]*School of Physics & Astronomy, University of St Andrews, North Haugh, St Andrews KY16 9SS*
[4]*Astrophysics Research Institute, Liverpool John Moores University, Twelve Quays House, Egerton Wharf, Birkenhead CH41 1LD*
[5]*Centre for Astronomy and Particle Theory, University of Nottingham, University Park, Nottingham NG7 2RD*
[6]*European Southern Observatory, Karl-Schwarzschild-Str. 2, 85748 Garching, Germany*
[7]*Astronomy Centre, University of Sussex, Falmer, Brighton BN1 9QH*
[8]*Institute for Astronomy, University of Edinburgh, Royal Observatory, Blackford Hill, Edinburgh EH9 3HJ*
[9]*Jeremiah Horrocks Institute, University of Central Lancashire, Preston PR1 2HE*
[10]*Max Planck Institute for Nuclear Physics (MPIK), Saupfercheckweg 1, 69117 Heidelberg, Germany*
[11]*Department of Physics, Swiss Federal Institute of Technology (ETH-Zürich), 8093 Zürich, Switzerland*
[12]*Institute for Computational Cosmology, Department of Physics, Durham University, South Road, Durham DH1 3LE*
[13]*Leiden University, PO Box 9500, 2300 RA Leiden, the Netherlands*
[14]*Carnegie Institution for Science, 813, Santa Barbara Street, Pasadena, CA 91101, USA*
[15]*Institute of Cosmology and Gravitation (ICG), University of Portsmouth, Dennis Sciama Building, Burnaby Road, Portsmouth PO1 3FX*
[16]*School of Physics, Monash University, Clayton, Victoria 3800, Australia*
[17]*Astronomy Unit, Queen Mary University London, Mile End Road, London E1 4NS*

Accepted 2010 August 25. Received 2010 August 17; in original form 2010 March 11

ABSTRACT

We present self-consistent star formation rates derived through pan-spectral analysis of galaxies drawn from the Galaxy and Mass Assembly (GAMA) survey. We determine the most appropriate form of dust obscuration correction via application of a range of extinction laws drawn from the literature as applied to Hα, [O II] and UV luminosities. These corrections are applied to a sample of 31 508 galaxies from the GAMA survey at $z < 0.35$. We consider several different obscuration curves, including those of Milky Way, Calzetti and Fischera & Dopita curves and their effects on the observed luminosities. At the core of this technique is the observed Balmer decrement, and we provide a prescription to apply optimal obscuration corrections using the Balmer decrement. We carry out an analysis of the star formation history (SFH) using stellar population synthesis tools to investigate the evolutionary history of our sample of galaxies as well as to understand the effects of variation in the initial mass function (IMF) and the effects this has on the evolutionary history of galaxies. We find that the Fischera & Dopita obscuration curve with an R_v value of 4.5 gives the best agreement between the different SFR indicators. The 2200 Å feature needed to be removed from this curve to obtain complete consistency between all SFR indicators suggesting that this feature may not be common in the average integrated attenuation of galaxy emission. We also find that the UV dust obscuration is strongly dependent on the SFR.

Key words: galaxies: evolution – galaxies: formation – galaxies: fundamental parameters – galaxies: general – galaxies: luminosity function, mass function.

⋆E-mail: d.wijesinghe@physics.usyd.edu.au

1 INTRODUCTION

The absorption of light by dust in galaxies presents a major challenge in measuring accurate star formation rates (SFRs) in galaxies. Understanding star formation is essential to our understanding of the evolutionary history of the Universe on both local and global scales. SFRs are commonly derived from Hα and ultraviolet (UV) luminosities, both of which are significantly affected by dust obscuration. The basic approach to correcting for this relies on having an observed constraint on the level of the attenuation, such as the Balmer decrement (Seaton 1979; Cardelli, Clayton & Mathis 1989; Calzetti 2001) or the β parameter (Calzetti, Kinney & Storchi-Bergmann 1994; Meurer, Heckman & Calzetti 1999; Adelberger & Steidel 2000) together with a model for the wavelength-dependence of the attenuation (Seaton 1979; Cardelli et al. 1989; Calzetti 2001; Pierini et al. 2004; Tuffs et al. 2004; Fischera & Dopita 2005, hereafter FD05).

Dust has the dual effect of not only reducing the overall luminosity observed from a galaxy but also imprinting wavelength-dependant spectral variations (Calzetti 1997a). Dust absorbs short-wavelength radiation and re-emits this energy at longer wavelengths. Dust also plays a significant role in the fluid dynamics, chemistry and star formation of galaxies (Draine et al. 2007). Even though dust plays a crucial role in galaxies, quantifying its effects and physical properties remains challenging. Understanding the roles played by inclination angles, optical depths and galaxy morphologies when coupled with dust has been even more difficult, and only recently have these effects been quantified by Tuffs et al. (2004).

Correcting for the effects of dust attenuation is usually done using semi-empirical models (see Cardelli et al. 1989; Byun, Freeman & Kylafis 1994; Calzetti 2001) but there are radiative transfer (RT) models developed for attenuation corrections (Xilouris et al. 1997; Xilouris, Alton & Davies 1998; Xilouris et al. 1999; Witt 1992; Tuffs et al. 2004). Even though modelling techniques can give more accurate attenuation corrections than semi-empirical models, they require more observational information about the galaxies in order to produce accurate corrections on an object-by-object basis. However, the RT techniques have proven extremely powerful when utilized to create libraries of model simulations (Tuffs et al. 2004) for use in statistical analysis of large statistical samples (Driver et al. 2009).

An important method for providing accurate SFRs is the spectral energy distribution (SED) modelling technique. There are two main types of SED techniques: template fitting SEDs (Calzetti et al. 2000; Salim et al. 2007) and RT SED techniques (Silva et al. 1998; Popescu et al. 2000). In particular, the accuracy of the RT SED techniques is high, but it tends to be complex and requires knowledge of the SED over the whole electromagnetic spectrum, from UV to far-infrared (FIR) and sub-millimetre wavelengths, which is not always available. Due to this complexity, the use of RT techniques is less favoured than empirical methods for dust correction.

Balmer decrements are commonly used as an indicator of obscuration corrections and are usually applied in conjunction with an extinction law such as those for the Milky Way (MW) (Nandy et al. 1975; Seaton 1979; Cardelli et al. 1989), Small Magellanic Cloud (SMC; Prévot et al. 1984; Bouchet et al. 1985), Large Magellanic Cloud (LMC; Fitzpatrick et al. 1986), and that observed for M31 (Bianchi et al. 1996), starburst galaxies (Calzetti 1997a, 2001) and other galaxies (FD05). Any extinction law can be used to correct either nebular emission lines or continuum emission. As a consequence of how these curves are derived, though, some curves are preferred over others to correct for each type of emission, as the processes that result in these two types of emission are different and it has been shown that nebular lines are usually obscured more than the continuum emission (Fanelli, OConnell & Thuan 1988; Calzetti, Kinney & Storchi-Bergmann 1994; Calzetti 1997b; Mas-Hesse & Kunth 1999). A physical interpretation for this is provided by Keel (1993) and Calzetti et al. (1994) who argue that the ionizing hot (young) stars which produce the nebular lines are found in or close to the dusty molecular clouds from which they were born, while the UV continuum is a product of older stars that have over time moved away from the dust clouds in which they formed, or have destroyed the dust in situ revealing the cluster of stars.

The obscuration curves are also dependent on their environments, in particular the metallicity of the host galaxy (Cardelli et al. 1989). For instance, the LMC, SMC and MW curves have a large variation in values at the FUV end of the spectrum due to the different metallicities of the three galaxies and grain size distribution (Calzetti et al. 1994; Calzetti 1997b) in the interstellar medium. These LMC, SMC and MW obscuration curves only take into account the dust between the observer and the star but in the case of external galaxies the dust geometry is more complicated. Not only does the dust between the observer and the stars of the galaxy need to be taken into account, but back-scattering of light into the line of sight from dust in other regions of the galaxy must also be considered and the dust is never uniformly distributed. The Calzetti extinction curve attempts to consider all these issues by folding a variety of obscuration effects into a single expression.

Meurer et al. (1999) show a relationship between the ratio of FIR and UV fluxes and the UV spectral slope β for a sample of starburst galaxies. Because this technique relates the FIR and UV radiation emitted from galaxies it can be a powerful tool in recovering the UV radiation lost due to the dust, regardless of the geometry of the dust. The β parameter is based on the relation between the gradient in the UV obscuration curve and the UV wavelengths (Meurer et al. 1999; Calzetti et al. 1994; Adelberger & Steidel 2000). However, this method is only recommended for starburst galaxies as quiescent galaxies tend to deviate from the total FIR to UV luminosity ratio and UV spectral slope relation seen for starbursts (Kong et al. 2004). The accuracy of this method is highly dependent on the method employed to measure the UV spectral slope. Calzetti et al. (1994) used 10 bands along the observed frame UV continuum spectrum avoiding all large-scale features that deviate from the trend of the slope. With large-scale surveys such as the Galaxy Evolution Explorer (GALEX) Medium Imaging Survey (MIS) this level of accuracy is unattainable, leading to less accurate measurements of the slope and potentially flawed dust corrections.

Once suitable dust corrections are in hand we can derive accurate SFRs and examine the relationship between galaxy properties and the dust content in a galaxy. SFRs are related to the luminosity through a linear scalefactor, determined with the assumption of a constant stellar initial mass function (IMF). These conversion factors will change if the IMF is varied. One recently suggested possibility is an evolving IMF (Wilkins, Trentham & Hopkins 2008a; Wilkins et al. 2008b; Gunawardhana et al. in preparation) which would lead to an evolving SFR conversion factor. Pflamm-Altenburg, Weidner & Kroupa (2009) proposed an Integrated Galaxy IMF (IGIMF) that combines the IMFs of all young-star clusters to form a galaxy-wide IMF. This was developed to account for the inconsistencies in current IMFs which are based on isolated stellar clusters and then applied on galaxy-wide scales. One of the inconsistencies that the IGIMF accounts for is the

discrepancy between FUV and Hα-derived SFRs at low SFRs (Sullivan et al. 2000; Lee et al. 2009).

We compare and contrast SFRs corrected for dust using different obscuration correction methods, identifying an optimum approach, and then use that in a preliminary investigation of SFR histories of galaxies. The SFRs are compared with theoretical evolutionary paths to better understand the star formation history (SFH) of the galaxies in our sample.

In Section 2, we present details of the data used. In Section 3, we present a prescription for the derivation and the application of the obscuration corrections. Section 4 compares Hα, FUV and [O II]-derived SFRs. Section 5 examines the evolution of our SFRs by comparing these SFRs to evolutionary synthesis models. We also compare the evolutionary paths of the SFRs with the predictions of the IGIMF theory. Section 6 is the summary and conclusion of our findings. The assumed cosmological parameters are as follows.

$H_0 = 70\,\mathrm{km\,s^{-1}\,Mpc^{-1}}$, $\Omega_\mathrm{M} = 0.3$ and $\Omega_\Lambda = 0.7$. All magnitudes are in the AB system.

2 DATA

We use data from the Galaxy and Mass Assembly (GAMA) survey (Driver et al. 2009). GAMA is a multi-band imaging and spectroscopic survey covering $\approx$144 deg^2 of sky in three $12^\circ \times 4^\circ$ regions (Robotham et al. 2009; Baldry et al. 2010). The spectroscopy comes from the AAOmega spectrograph (Sharp et al. 2006) at the Anglo Australian Telescope (AAT).

The UV data were obtained from the GALEX-GAMA survey (Seibert et al., in preparation). A signal-to-noise ratio cut of 2.5 was applied to the UV data. There are 111 521 GALEX sources within the GAMA regions of which 110 443 matching sources were found using a matching radius of 6 arcsec. Such a large matching radius is necessary due to the increased positional uncertainty inherent in the larger GALEX point spread function (PSF). SDSS and spectral-line data were matched to GAMA sources using a matching radius of 2.5 arcsec resulting in a final sample of 47 269 objects. After removing AGN (using the prescription of Kewley et al. 2001) and sources without emission lines, r-band magnitude and redshift data the final sample size contained 31 508 galaxies. All remaining galaxies contain both Hα and Hβ fluxes. The final sample has a GALEX FUV magnitude range of $14.7 < m_\mathrm{FUV} < 25.3$ and a redshift limit of $z < 0.350$ due to the requirement for Hα being in the observed spectral range.

3 DUST OBSCURATION CORRECTIONS

Correcting galaxy emission for dust requires a case-specific approach, that is nebular and continuum emission from galaxies require two different treatments. At the core of these obscuration corrections are the obscuration curves and the Balmer decrement. We apply several different obscuration curves to examine their effects on continuum (UV) and nebular (Hα and [O II]) emission.

3.1 Continuum emission corrections

Applying obscuration corrections for continuum emission requires two parts, the reddening suffered by the stellar continuum [$E(B-V)_\mathrm{cont}$] and an applicable obscuration curve ($k(\lambda)$). We use the standard form

$$L_\mathrm{i} = L_\mathrm{o} 10^{0.4E(B-V)_\mathrm{cont}k(\lambda)} \quad (1)$$

to apply our dust corrections. L_i and L_o are the intrinsic and observed galaxy luminosities, respectively. To obtain $k(\lambda)$ for the UV stellar continuum, the Calzetti (2001) obscuration curve and the FD05 obscuration curves can be applied. When using the Calzetti (2001) curve $k(\lambda)$ must be divided by 0.44. The FD05 curves can also be applied to correct for the obscuration of nebular emission. The UV luminosities were derived using the UV fluxes from the GALEX survey and the redshifts obtained from the GAMA survey.

$E(B-V)_\mathrm{cont}$ is derived from the reddening in the ionized gas, $E(B-V)_\mathrm{gas}$. $E(B-V)_\mathrm{cont} = 0.44E(B-V)_\mathrm{gas}$ (Calzetti 2001) and

$$E(B-V)_\mathrm{gas} = \frac{\log\left(\frac{f_{H\alpha}}{f_{H\beta}}/2.86\right)}{0.4[k(\mathrm{H}\beta) - \mathrm{k}(\mathrm{H}\alpha)]}, \quad (2)$$

where $k(\mathrm{H}\beta)$ and $k(\mathrm{H}\alpha)$ are the obscurations of the nebular emission at the Hα and Hβ wavelengths derived from an MW obscuration curve (Seaton 1979; Cardelli et al. 1989) or a theoretically modelled curve (FD05) as in this paper. $f_{\mathrm{H}\alpha}$ and $f_{\mathrm{H}\beta}$ are the stellar absorption-corrected but not dust-corrected Hα and Hβ fluxes.

$f_{\mathrm{H}\alpha}$ and $f_{\mathrm{H}\beta}$ were corrected for stellar absorption using the formalism outlined in Hopkins et al. (2003) stated below.

$$f_s = \left[\frac{\mathrm{EW} + \mathrm{EW_c}}{\mathrm{EW}}\right] f_\mathrm{o}, \quad (3)$$

where f_o and f_s are the observed and stellar absorption corrected fluxes, respectively. EW is the equivalent width of the line being corrected and $\mathrm{EW_c}$ is the correction for stellar absorption taken to be 0.7 Å which has been shown to be a reasonable assumption (Gunawardhana et al., in preparation).

Assuming a Case-B recombination with a density of $100\,\mathrm{cm^{-3}}$ and a temperature of 10 000 K, the predicted ratio of $f_{\mathrm{H}\alpha}$ to $f_{\mathrm{H}\beta}$ is 2.86 (Osterbrock 1989). All Balmer decrements below 2.86 were set equal to 2.86 as suggested by Kewley (2006). We applied k-corrections to the observed GALEX UV magnitudes, using KCORRECT.v4.1.4 (Blanton et al. 2003) to infer the rest-frame magnitude in each GALEX band, with effective wavelengths of 1528 and 2271 Å, before the dust correction process.

It is important to note that correcting continuum emission for dust using this technique requires both MW and continuum obscuration curves. MW obscuration curves such as in Seaton (1979) and Cardelli et al. (1989) are required for the derivation of $E(B-V)_\mathrm{cont}$ while a continuum obscuration curve such as in Calzetti (2001) provides $k(\lambda)$.

A theoretically modelled curve such as FD05 is applicable to both the nebular and continuum components. The reason for this is that unlike the other extinction correction curves, these curves were derived from dust models that do not require assumptions about the effects of the emission sources of the galaxy. The model is based on the inferred physical properties of the turbulent density structure (FD05). The FD05 curves are described for a range of R_v values, and we examine the effects of different R_v values. $R_v = A_V/E(B-V)_\mathrm{gas}$, where A_V is the extinction suffered in the rest-frame V band.

3.2 Nebular emission-line corrections

To correct Hα emission for dust, the Hα luminosity needs to be calculated first. Hα luminosities corrected for stellar absorption, taking into account aperture corrections, can be obtained using the formalism outlined in Hopkins et al. (2003),

$$L_{\mathrm{H}\alpha} = (\mathrm{EW}_{\mathrm{H}\alpha} + \mathrm{EW_c})10^{-0.4(M_r - 34.10)} \frac{3 \times 10^{18}}{[6564.61(1+z)]^2}. \quad (4)$$

M_r is the k-corrected absolute r-band AB magnitude. The last factor converts units from W Hz^{-1} to W Å^{-1} and 6564.61 Å is the vacuum wavelength of Hα.

Aperture corrections account for the fact that only a limited amount of emission from a galaxy is detected through the 2 arcsec diameter AAOmega fibre. The aperture correction implicitly assumes that the emission measured through the fibre is characteristic of the whole galaxy, and that the star formation is traced by the *r*-band continuum emission (Hopkins et al. 2003).

Obscuration corrections are then applied to the Hα luminosity as follows:

$$L_{\rm i} = L_{\rm H\alpha}\left(\frac{f_{\rm H\alpha}/f_{\rm H\beta}}{2.86}\right)^{2.942}. \quad (5)$$

The exponent in the above equation is derived from the FD05 ($R_v = 4.5$) extinction curve and will vary according to the (MW) obscuration curve. This form of obscuration correction has the same end result as

$$L_{\rm i} = L_{\rm H\alpha}10^{0.4E(B-V)_{\rm gas}k(\lambda)}. \quad (6)$$

In this case, $k(\lambda)$ can be derived from an MW obscuration curve such as Seaton (1979), Cardelli et al. (1989) or a theoretically modelled curve such as FD05.

An analogous method can be used to derive [O II] luminosities but the stellar absorption correction ($\rm EW_c$) is not required. M_r is replaced by M_u and the Hα wavelength is replaced by the [O II] doublet effective wavelength, 3728.30 Å (Hopkins et al. 2003). As in the case of Hα, aperture corrections are included but obscuration corrections are not.

$$L_{\rm [O\,II]} = {\rm EW}_{\rm [O\,II]}10^{-0.4(M_u-34.10)}\frac{3\times10^{18}}{[3728.30(1+z)]^2}. \quad (7)$$

[O II] emission can be used as an SFR estimator, particularly at high redshifts (Gilbank et al. 2010). The [O II] emission must be corrected for obscuration based on the obscuration at the wavelength of Hα so that the SFR calibration derived for Hα luminosities (calibrated to [O II]) can be used (Kennicutt 1992, 1998; Hopkins et al. 2003).

3.3 β parameter

The β parameter (Meurer et al. 1999; Adelberger & Steidel 2000) has been proposed in order to provide obscuration corrections for starburst galaxies when the Balmer decrement is not available. It is derived from the relationship between the UV spectral slope and UV to FIR flux ratio.

The β parameter is the UV spectral slope determined from a power-law fit to the UV continuum of the form

$$f_\lambda \propto \lambda^\beta, \quad (8)$$

where f_λ is the flux density per wavelength interval and λ is the central rest wavelength (Meurer et al. 1999). The relationship between the β parameter and the ratio of FIR and UV fluxes is used to account for dust in galaxies. Calzetti et al. (1994) recommend observing the UV continuum bands that avoid irregularities along the UV spectral slope that would alter the gradient of the slope that is measured. In our case only two UV bands are available, those of far-UV (FUV) and near-UV (NUV) from the GALEX satellite that span 1400–1800 Å and 1800–2800 Å with effective wavelengths $\lambda_{\rm FUV} = 1528$ Å and 2271 Å, respectively.

Due to the poor sampling of the underlying UV spectrum by the broad GALEX UV bands, and significant contamination by local structure across these bands the accuracy with which the UV slope can be determined is compromised. Kong et al. (2004) state that this definition of β does not apply to galaxies for which only multi-band UV imaging is available, as in the case with GALEX MIS Survey. Instead Kong et al. (2004) recommend the definition

$$\beta = \frac{\log\bar{f}_{\rm FUV} - \log\bar{f}_{\rm NUV}}{\log\lambda_{\rm FUV} - \log\lambda_{\rm NUV}}, \quad (9)$$

where $\lambda_{\rm FUV} = 1528$ and $\lambda_{\rm NUV} = 2277$ are the effective wavelengths of the FUV and NUV filters of the GALEX satellite. $\bar{f}_{\rm FUV}$ and $\bar{f}_{\rm NUV}$ are the mean flux densities per unit wavelength through these filters. We aim to compare the dust corrections from this technique with corrections made using the Balmer decrement. This would allow us to observe the effect that the β parameter will have on dust corrections in our sample of largely quiescent galaxies.

The UV luminosities are corrected for starburst galaxies using the relation $A_{1600} = 4.43 + 1.99\beta$ from Meurer et al. (1999), where A_{1600} is the attenuation at 1600 Å:

$$L_{\rm i} = 10^{0.4(4.43+1.99\beta)}L_{\rm o}, \quad (10)$$

where $L_{\rm i}$ and $L_{\rm o}$ are the FUV dust corrected and uncorrected luminosities.

We apply this formalism to our sample of largely quiescent galaxies to test the extent to which β and hence the corrected luminosities and SFRs are overestimated as Kong et al. (2004) have suggested.

4 COMPARISON OF STAR FORMATION RATES

Star formation rates can be calculated from scaling factors applied to the luminosities. The scaling factors are dependent on the IMF used (Salpeter 1955; Kennicutt 1983). We use a Baldry & Glazebrook (2003) IMF with a mass range of 0.1 $\rm M_\odot$ to 120 $\rm M_\odot$. The effects of applying other IMFs (Salpeter 1955; Kennicutt 1983; Scalo 1998) are explored in Section 4. For Hα, FUV and NUV luminosities the SFR conversion factors were calculated using a population synthesis model (PEGASE.2; Fioc & Rocca-Volmerange 1997).

The [O II] SFR conversion factor was derived from the flux ratio of [O II] and Hα, where $F_{\rm [O\,II]}/F_{\rm H\alpha} = 0.23$ (Hopkins et al. 2003) and the Hα SFR conversion factor (Kennicutt 1992). A stellar absorption correction of 0.7 Å (Gunawardhana et al., in preparation) is applied before this ratio is obtained. The luminosity to SFR calibration for [O II] can be calculated in this way because the SFRs come from using the [O II] emission as a proxy for the Hα emission. SFRs derived from [O II] luminosities are based on the fact that there is a good correlation between *observed* [O II] and Hα line fluxes (Kennicutt 1992, 1998; Hopkins et al. 2003).

For FUV, NUV, Hα and [O II] luminosities, SFRs can be calculated using linear scalefactors, derived using PEGASE, as follows:

$${\rm SFR_{FUV}}(\rm M_\odot\,yr^{-1}) = \frac{L_{\rm FUV}}{1.64\times10^{21}\,W\,Hz^{-1}} \quad (11)$$

$${\rm SFR_{NUV}}(\rm M_\odot\,yr^{-1}) = \frac{L_{\rm NUV}}{1.56\times10^{21}\,W\,Hz^{-1}} \quad (12)$$

$${\rm SFR_{[O\,II]}}(\rm M_\odot\,yr^{-1}) = \frac{L_{\rm [O\,II]}}{7.967\times10^{33}\,W} \quad (13)$$

$${\rm SFR_{H\alpha}}(\rm M_\odot\,yr^{-1}) = \frac{L_{H\alpha}}{3.464\times10^{34}\,W}. \quad (14)$$

These SFR conversion factors are consistent with those of Kennicutt (1998) for Hα, Hopkins et al. (2003) for [O II] and Madau, Pozzetti & Dickinson (1998) for UV, when taking into account the choice of IMF (Baldry & Glazebrook 2003).

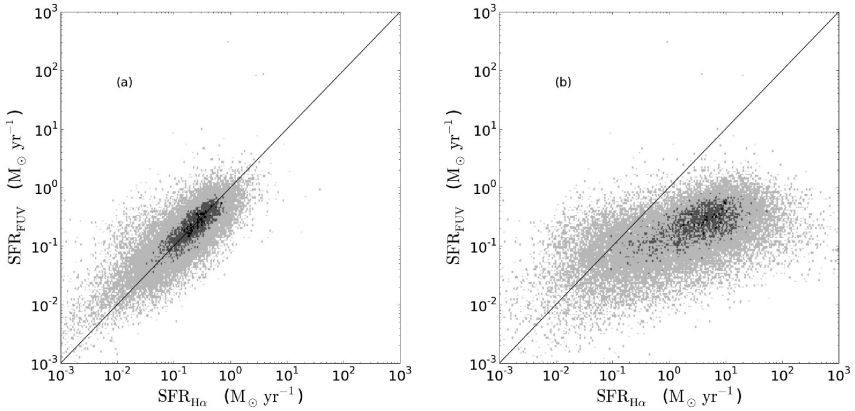

Figure 1. SFR derived from FUV luminosity as a function of SFR derived from Hα luminosity. All galaxies in our sample are shown, with AGNs excluded. (a) Both SFR indicators without obscuration corrections, and (b) only the Hα-derived SFRs are corrected for dust obscuration using an FD05 curve with an R_v value of 4.5. The axis ranges in the above panels, and subsequent figures, are the same for ease of comparison. The strong luminosity dependence of the obscuration corrections is clear (Hopkins et al. 2001, 2003; Afonso et al. 2003).

Fig. 1(a) shows the FUV SFRs as a function of Hα SFRs with both indicators uncorrected for dust obscuration, and Fig. 1(b) shows the same but with only the Hα SFRs corrected for dust obscuration. This shows the effect that obscuration corrections have on the luminosity and how the observed and intrinsic luminosities compare. In Fig. 1, when dust corrections are applied (in this case only to the Hα), the SFR values of high SFR objects increase by $\approx$2 orders of magnitude. At low SFRs the distribution remains close to the one-to-one line. From similar analyses of uncorrected FUV and Hα SFRs by Sullivan et al. (2000) and Lee et al. (2009), it is clear that our data follow similar trends. Even at high SFR, it is clear that our SFRs are a continuation of the same trends observed in Sullivan et al. (2000) at lower SFRs.

Figs 2 (FUV) and 3 (NUV) show the relationship between Hα, FUV and NUV SFRs after the luminosities have been corrected for dust obscuration by various obscuration curves. Fig. 4 shows a similar comparison between Hα and [O II] SFRs. The obscuration curves are compared in Fig. 5. There is an overestimation of the UV SFRs when only using the Cardelli et al. (1989) curve for both the Hα and UV corrections (Figs 2a and 3a). The overestimation is larger at higher SFRs. A similar overestimation is seen when only the Calzetti (2001) curve is used to correct both Hα and UV SFRs (Figs 2b and 3b). The overestimation is constant for all SFRs.

Figs 2(c) and 3(c) show SFRs after the dust corrections were carried out on the appropriate type of emission. This means that when dust correcting FUV and NUV luminosities, an MW obscuration curve (Cardelli et al. 1989) was used for the nebular emission parts of UV dust correction and a Calzetti (2001) curve was used for the continuum parts of UV dust correction as outlined in Section 3.1. The Hα luminosities were corrected using the same MW obscuration curve (Cardelli et al. 1989) that was used for the nebular emission correction part of the UV dust corrections. There is still an overestimation in the UV and this overestimation is larger than that in panels (a) and (b) in Fig. 2 and panel (b) in Fig. 3. The overestimation is larger at the high SFR end for both FUV and NUV.

In panels (d), (e) and (f) in Fig. 2, the same FD05 curve (i.e. the same R_v value) is used for nebular and continuum parts of UV dust correction and for the dust correction of Hα for each panel. There is good agreement between Hα and FUV-derived SFRs for an R_v value of 4.5 (Fig. 2 e). This value also agrees with the R_v value suggested by Calzetti (2001) as well as comparisons made between FD05 curves and the Calzetti (2001) curve (Fischera, Dopita & Sutherland 2003). For R_v values less than 4.5, the FUV SFRs are overestimated (Fig. 2d; $R_v = 3.5$) and for values above 4.5 the FUV SFRs become underestimated (Fig. 2f; $R_v = 5.5$), with respect to the Hα SFRs. Both Hα and FUV luminosities were corrected using the same FD05 curve.

The corrections applied to the NUV SFR using the FD05 extinction curves only lead to an agreement with Hα SFRs at an R_v value of 6 (Fig. 3f). Applying an R_v value of 4.5 that is consistent with FUV dust corrections overestimates the NUV SFRs, as shown in Fig. 3(d). R_v values higher than 6 lead to an underestimation of NUV SFRs while lower values lead to an overestimation in the NUV SFRs. Not only is $R_v = 6$ inconsistent with the value obtained for the matching between Hα and FUV SFRs, it is also too high to be a realistic value (Seaton 1979; Cardelli et al. 1989; Calzetti 2001). The answer to this dilemma lies in the Cardelli et al. (1989) curve. This obscuration curve overcorrects the NUV-derived SFRs more than the FUV-derived SFRs. A similar result is obtained when the Seaton (1979) obscuration curve is used.

In comparing Figs 2 and 3, the Calzetti (2001) obscuration curve [used in panel (b) in both figures] is the only obscuration curve that does not overcorrect NUV more than FUV. This is due to the inclusion of the 2200 Å feature in the MW and FD05 extinction curves which magnifies the dust corrections. This feature is present in all the curves that are discussed here except for the Calzetti (2001) curve. The sudden increase in the extinction correction near NUV wavelengths is undoubtedly the source of the overcorrection seen in Fig. 3. For this reason, we calculated the NUV dust correction using an FD05 curve with an R_v value of 4.5 but interpolating across the 2200Å feature (as shown in Table 1, where A_v is the total attenuation). The results seen in Fig. 3(d) are very promising. The Hα and NUV SFRs are very closely matched, however, there appears to be a slight overestimation in the NUV SFRs at all SFRs. This is a result of the interpolation technique used to recreate this obscuration curve without the 2200 Å feature. We find that to correct NUV luminosities for the effects of dust, the role of the 2200 Å feature will have to be reassessed. The implication is that the 2200 Å feature is a property of MW dust grains that does not seem to propagate to the global integrated attenuation properties of galaxies.

Fig. 4 shows a good correlation between Hα and [O II] derived SFRs. Both the FD05 ($R_v = 4.5$) and Cardelli et al. (1989) curves show good agreement between Hα and [O II] SFRs as seen in Fig. 4.

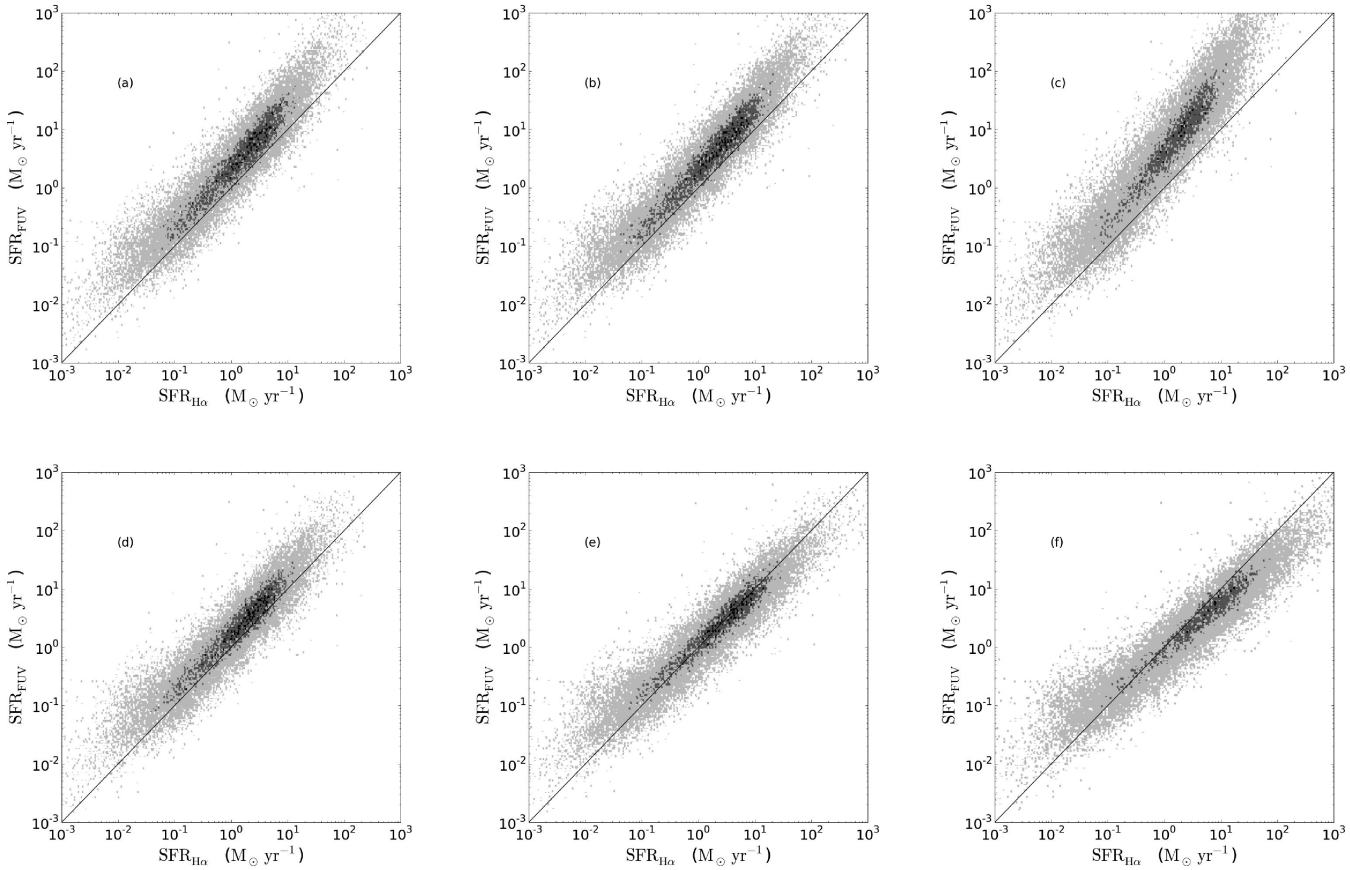

Figure 2. FUV SFRs as a function of Hα SFRs, dust-corrected with a variety of obscuration corrections. Both Hα and FUV luminosities are corrected with consistent obscuration curves as described in the text. (a) A Cardelli et al. (1989) extinction curve is used to correct both Hα and FUV luminosities. (b) A Calzetti (2001) curve corrects both Hα and FUV luminosities. (c) Cardelli et al. (1989) and Calzetti (2001) curves correct for the nebular and continuum emission, respectively. (d), (e) and (f) show SFR values corrected using FD05 extinction curves with R_v values of 3.5, 4.5 and 5.5, respectively, for both luminosities. The best agreement between Hα and FUV-derived SFRs is the FD05 extinction curve with an R_v value of 4.5 (panel e).

Fig. 4(a) indicates that [O II] luminosities are obscured more than Hα as the Hα SFRs are larger than [O II] before the dust corrections. This is expected as shorter wavelengths are more sensitive to dust obscuration. We find that the metallicity dependence of the [O II] SFRs does not play a significant role in biasing the SFRs derived from [O II] for this sample although it may contribute to the observed scatter. It may become significant for the low-SFR systems which begin to deviate from the one-to-one line in Fig. 4 (Kewley et al. 2001).

Finally, we turn to an investigation of the utility of the β parameter for making obscuration corrections to UV-derived SFRs. As mentioned above, β is demonstrated to be a useful obscuration parameter only for starburst galaxies (Kong et al. 2004). Our sample consists of galaxies with a broad range of SFRs, but containing very few starbursts. The distribution of stellar-mass doubling-times, $t_{\rm d}$, ranges from 10^8 to 10^{13} yr, with the vast majority (≈97 per cent) having $t_{\rm d} > 10^9$. The definition of a starburst is such that their mass doubling times should be less than ≈1 Gyr, so even the very high SFR systems in our sample (in particular) are not starbursts, as they are also among the most massive.

Our results (Fig. 6) clearly show FUV SFRs, corrected for obscuration using β, that are significantly overestimated, by up to two orders of magnitude when compared to Hα-derived SFRs corrected using the FD05 curve. As Kong et al. (2004) suggest, when the β parameter is applied to non-starburst galaxies the value of β will be overestimated, leading to an overestimation in the dust present in the galaxy and consequently the inferred SFR.

Panel (b) of Fig. 6 shows FUV-derived SFRs corrected using a modified β attenuation correction to that of Meurer et al. (1999). The corrected attenuation factor was derived from the offset seen in FUV-derived SFRs compared to Hα SFRs when the attenuation factor of Meurer et al. (1999) is used to correct FUV luminosities. We describe the attenuation as

$$A = 3.3 + 1.99\beta. \quad (15)$$

The galaxies in Fig. 6(b) do appear somewhat more evenly distributed on either side of the one-to-one line. There remains, though, a very large scatter, with an rms of 0.27.

The conversion from luminosities to SFRs is carried out with the assumption that the IMF is constant and independent of the total SFR. Evolving IMFs could have an impact on the way luminosities are converted into SFRs, affecting the trends observed so far, but addressing this is deferred to later publications.

5 SFR HISTORY

The SFR distributions shown in the previous section include galaxies at various stages of their evolution. By comparing these galaxies with evolutionary synthesis models, using PEGASE.2 (Fioc & Rocca-Volmerange 1997), we can develop an understanding of the

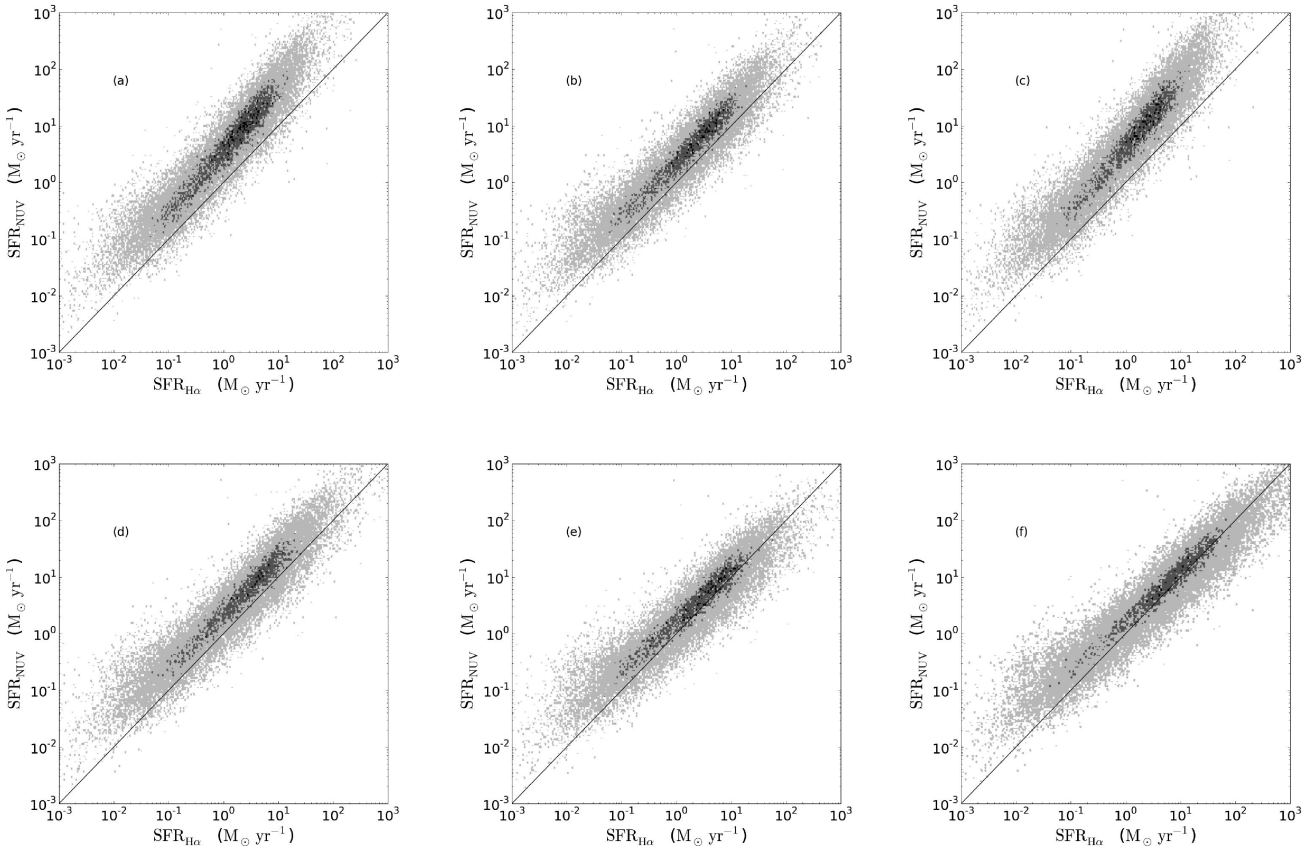

Figure 3. NUV SFRs as a function of Hα SFRs dust corrected with a variety of obscuration corrections. Both Hα and NUV luminosities are corrected with consistent obscuration curves. (a) A Cardelli et al. (1989) curve was used to correct both Hα and NUV luminosities. (b) A Calzetti (2001) curve corrects for both Hα and NUV luminosities. (c) Cardelli et al. (1989) and Calzetti (2001) curves correct for the nebular and continuum emission, respectively. (d) An FD05 curve with an R_v value of 4.5 and with the 2200 Å feature is used to correct both Hα and NUV. (e) An FD05 curve with an R_v value of 4.5 and without the 2200 Å feature is used to correct both Hα and NUV. (f) An FD05 curve with an R_v value of 6 and with the 2200 Å feature is used to correct both Hα and NUV. The best agreement between Hα- and NUV-derived SFRs is when the FD05 extinction curve with an R_v value of 6 (panel f), and 4.5 without the 2200Å feature (panel e), are used. This result is at odds with that of Fig. (2) as the extinction curves are not consistent between FUV and NUV luminosities unless we remove the 2200Å feature.

Table 1. Modified FD05 curve ($R_V = 4.5$) without the 2200 Å feature.

λ μm	k_λ
0.0192	$8.133 + R_V$
0.1503	$6.932 + R_V$
0.1216	$5.621 + R_V$
0.1550	$4.169 + R_V$
0.3000	$2.684 + R_V$
0.3650	$1.830 + R_V$
0.4400	$1.000 + R_V$
0.5480	$0.000 + R_V$
0.7200	$-1.134 + R_V$
1.0300	$-2.323 + R_V$
1.2390	$-2.786 + R_V$
1.6490	$-3.336 + R_V$
2.1920	$-3.714 + R_V$
3.5920	$-4.179 + R_V$
4.7770	$-4.130 + R_V$

effects that various galaxy parameters have on their evolution and even explain some of the trends and scatter observed in our data. The output of the evolutionary synthesis model is normalized to a galaxy of one solar mass. To compare the theoretical models with the observed data we must scale the theoretical output according to the mass of the galaxies we are analysing.

The galaxy mass is derived using the *g*- and *i*-band colours and the absolute magnitude in the *i*-band ($M_{\rm i}$).

$$M_* = 10^{1.04+0.9(g-i)-0.4M_{\rm i}}, \quad (16)$$

where *g* and *i* refer to the SDSS Petrosian magnitudes observed in the *g* and *i* bands (Baldry et al. 2004; Talor et al. 2009).

Fig. 7 shows how the modelled evolutionary paths compare to the observed measurements. The paths in Fig. 7 have a Baldry & Glazebrook (2003) IMF and an exponentially declining SFR with $\tau = 90$ Myr. To give an indication of time on the evolutionary paths, the evolutionary paths begin at 0 Myr and are displayed to $\approx$1000 Myr in Fig. 8. The evolutionary paths indicate that the FUV-derived SFRs and Hα-derived SFRs should strongly agree at all the SFRs that we have obtained. For the case of Hα and FUV SFRs this is consistent with our measurements.

For the majority of the galaxies we compare, the masses of observed galaxies and those of the evolutionary paths seem to agree at the ages of 200 to 500 Myr. In Fig. 8, these ages on the evolutionary paths correspond, given the exponentially declining SF histories, to SFRs ranging from 10^1 to 10^{-2} M$_\odot$ yr^{-1}. This is consistent across all mass scales in Fig. 7. The masses of the modelled paths and the observed data do not agree at younger ages indicating that we do

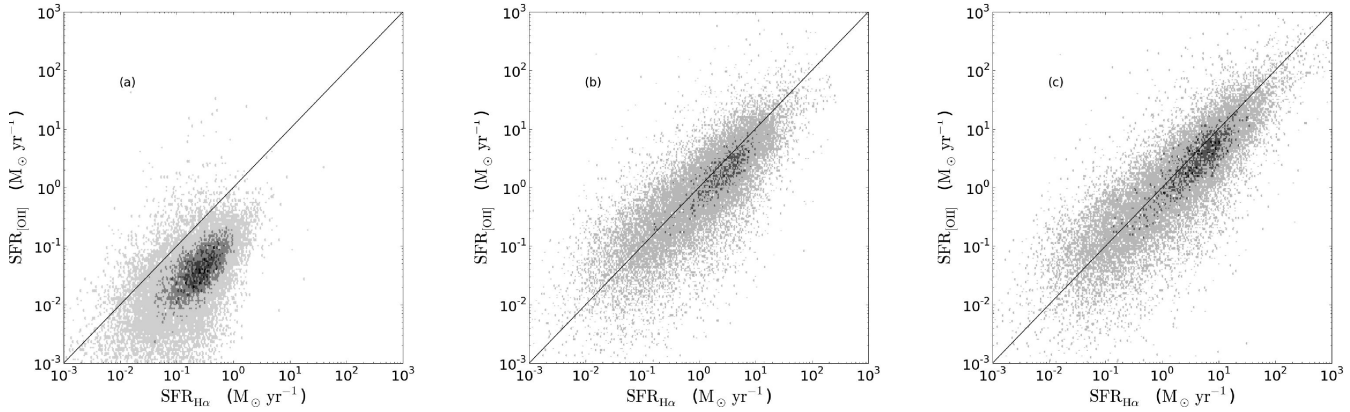

Figure 4. [O II] SFRs as a function of Hα SFRs. The [O II] luminosities were corrected based on the extinction at the Hα wavelength. (a) compares the SFR indicators without any extinction corrections. (b) compares SFRs obscuration corrected with the Cardelli et al. (1989) obscuration curve. (c) compares SFRs obscuration corrected with the FD05 obscuration curve with an R_v value of 4.5.

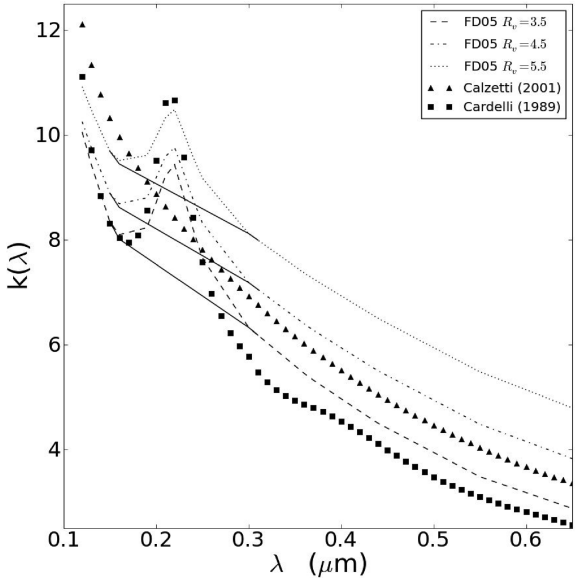

Figure 5. The Cardelli et al. (1989), Calzetti (2001) and FD05 ($R_v = 3.5$, 4.5, 5.5) obscuration curves. The three unbroken lines show the FD05 curves with the 2200 Å feature removed. It must be noted that the Calzetti (2001) curve is the only curve intrinsically without the 2200 Å feature.

not observe these galaxies at the earliest stages of their lives. Particularly the 'hook' like path seen at the early stages (<200 Myr) is not observed in our data and does not seem to constitute any of the scatter. At the older end, the masses of the models and the observed galaxies agree up to about 500 Myr.

Fig. 8(a) shows that different IMFs can produce different evolutionary paths particularly early in the life of a galaxy. The Baldry & Glazebrook (2003) IMF begins at a higher SFR, and using a Baldry & Glazebrook (2003) IMF will result in a galaxy at a particular age being observed to have a higher SFR compared to Salpeter (1955), Kennicutt (1983) or Scalo (1998) IMFs. The modelled paths assume a galaxy mass of 10^9 $\mathrm{M}_\odot$ with a 90 Myr characteristic decay time. All the IMFs share similar paths with the Baldry & Glazebrook (2003) IMF showing a better fit to the observed trend than the other three IMFs. The tracks assuming Salpeter (1955), Kennicutt (1983) and Scalo (1998) IMFs follow similar trends at almost the same rate

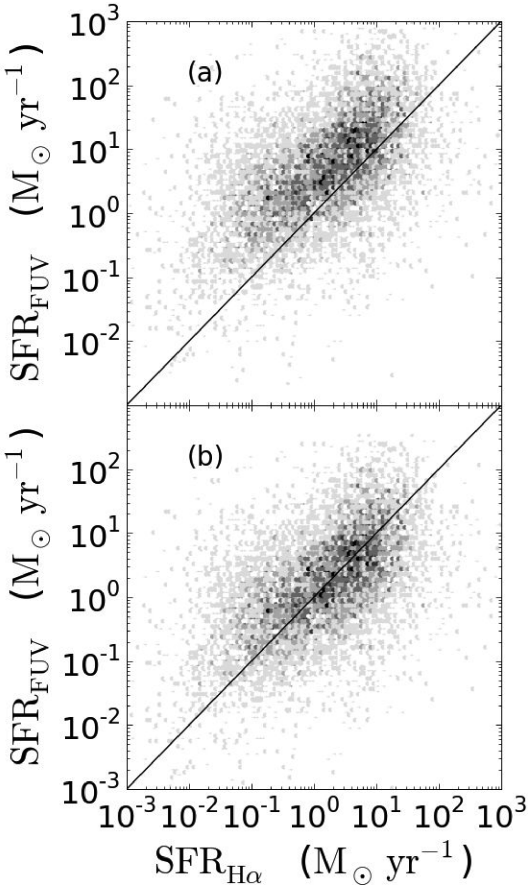

Figure 6. The figure compares the Hα-derived SFR, extinction corrected using an FD05 extinction curve ($R_v = 4.5$), against FUV-derived SFRs extinction corrected using the β parameter. (a) The FUV SFR corrected using the attenuation factor in Meurer, Heckman and Calzetti (1999). (b) The same as (a) but with FUV SFRs corrected for dust using a modified attenuation factor to that of Meurer, Heckman and Calzetti (1999) chosen to fit the one-to-one line. There is a large scatter with an overestimation of the FUV SFRs.

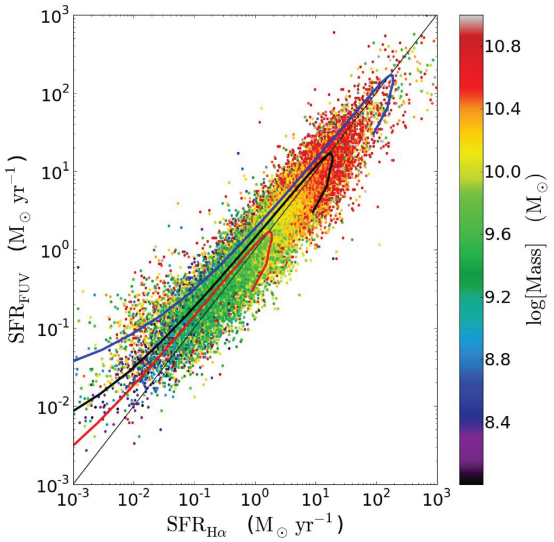

Figure 7. FUV SFRs as a function of Hα SFRs compared with PEGASE evolutionary models of galaxies with various masses. The colour scale represents the measured masses of the galaxies. The regions where the modelled paths agree with the observed masses give an indication of the ages of the galaxies in each part of each curve. The evolutionary paths are for exponentially decaying SFRs with masses of 10^8 M$_\odot$ (red), 10^9 M$_\odot$ (black) and 10^{10} M$_\odot$ (blue). All paths have a characteristic decay time of 90 Myr and a Baldry & Glazebrook (2003) IMF.

of evolution. The evolutionary paths for the IMFs match with the observed values at about the age of 130 Myr.

Also of interest is the lower SFR end where the evolutionary paths drift away from the one-to-one line and towards higher FUV-derived SFRs. This is clearly visible in the modelled evolutionary tracks. Even though our data do not extend below 10^{-2} M$_\odot$ yr^{-1} there is a mild but definite trend towards higher FUV SFRs compared to Hα SFRs observed at the low SFR end. By varying the characteristic decay times of the evolutionary paths, as in Fig. 8(b), various turn-off points can be modelled. A characteristic decay time of 90 Myr seems to agree well with the observed values. Possible causes for this behaviour will be discussed in Section 6.

Figs 7 and 8 show good model agreement with the observed SFR distributions. It is clear that the evolution of galaxies with 10^{-2} M$_\odot$ yr^{-1} < SFR < 10^2 M$_\odot$ yr^{-1} can be modelled effectively.

6 DISCUSSION

6.1 Obscuration curves

We have presented an analysis of the dust corrections in a sample of 31 058 galaxies from the GAMA survey. We analysed several techniques used to correct for the dust obscuration in galaxies.

The Calzetti formalism using the Calzetti (2001) obscuration curve has been deemed to be one of the best for applying obscuration corrections to FUV emission in starburst galaxies, but we find that in our sample of non-starburst galaxies, it overestimates the UV SFR. We find that a theoretically modelled obscuration mechanism by FD05 provides SFRs well-matched between FUV and Hα. In addition, we use a Balmer decrement to derive the colour excess suffered by the stellar continuum, $E(B-V)_{\rm star}$, to complete our UV dust corrections.

The effect of applying dust corrections is shown in Fig. 1 where the large increase in SFRs after applying dust corrections (to the Hα emission in this case) is a consequence of high star formation rate galaxies having much higher dust obscuration levels (Calzetti 2001; Hopkins et al. 2001, 2003; Afonso et al. 2003; van den Bergh 2007). The same figure illustrates the lack of dust in low star-forming systems as galaxies at the very low SFR end maintain similar SFRs after dust corrections.

We explored several obscuration curves used to correct emission line luminosities, such as the Seaton (1979) and Cardelli et al. (1989) MW obscuration curves as well as the FD05 curves. It is important that the appropriate type of obscuration curve is applied for different types of emission. The FUV emission from galaxies contains contributions from older and lower mass stellar populations (Bell 2003) which would have gradually moved away from the clouds of gas that formed them, whereas Hα and [O II] lines are emitted from the [H II] regions ionized by hot young stars that are contained within those clouds of gas. For this reason, different absorption curves could potentially apply to stellar and nebular emission, highlighting the importance of using the correct obscuration curve for each type of emission.

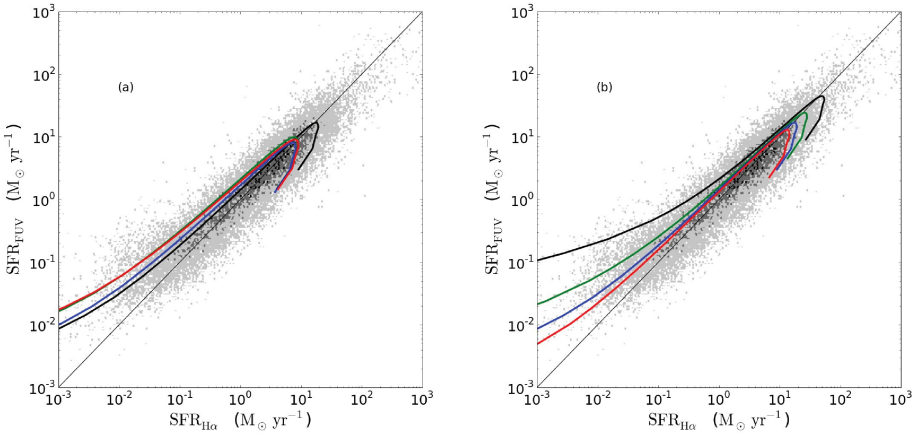

Figure 8. FUV SFRs as a function of Hα SFRs compared with PEGASE evolutionary models for different IMFs (panel a), and characteristic decay times (panel b). (a) Salpeter (1955) (blue), Kennicutt (1983) (green), Scalo (1998) (red) and Baldry & Glazebrook (2003) (black) IMFs are shown. All IMFs are scaled to a galaxy of mass 10^9 M$_\odot$ and a characteristic decay time of 90 Myr. (b) Characteristic decay times of 30 Myr (black), 60 Myr (green), 90 Myr (blue) and 120 Myr (red). All paths were derived using a Baldry & Glazebrook (2003) IMF scaled to a galaxy of mass 10^9 M$_\odot$.

This is clearly illustrated in Figs 2(a) and 3(a) where using the Cardelli et al. (1989) curve for both Hα and UV overestimates the UV SFRs. The Cardelli et al. (1989) curve is appropriate for correcting nebular emission, and is more likely to overcorrect for dust when applied to the UV stellar continuum.

The overestimation of the UV SFRs when the Calzetti (2001) curve is used (Figs 2b, c, 3b and c) can have several explanations. As highlighted by Calzetti, (Calzetti 2001), this curve is only applicable to starburst galaxies. It was also based on a small sample of 37 starburst galaxies using a universal extinction as opposed to a galaxy-specific approach. It must be noted that a starburst galaxy is not the same as a high SFR galaxy. A starburst galaxy requires a short mass-doubling time compared to a non-starburst galaxy reflecting an atypically high SFR. Most of the galaxies in our sample have mass doubling times consistent with not being in starburst mode. For this reason, it is conceivable that the Calzetti (2001) obscuration corrections would overestimate the UV-derived SFR of the galaxies in our sample. The processes that lead to starbursts such as interaction of galaxies, tidal shear in the solid body rotation and secular evolution of bars (Larson & Tinsley 1978; Sanders et al. 1988; Kennicutt 1990; Kenney, Carlstrom & Young 1993; Norman, Hasan & Sellwood 1996) would not necessarily occur in non-starburst galaxies and hence the spectral output can be different to a starburst galaxy.

The FD05 extinction curve, with an R_v value of 4.5, is successful in providing matching Hα, FUV and [O II]-derived SFRs at all SFRs that we have tested ($10^{-2}\,M_\odot\,yr^{-1} < SFR < 10^2\,M_\odot\,yr^{-1}$). An R_v value of 4.5 agrees with values prescribed by Calzetti (2001). The FD05 curves are theoretical models based on the physical density of the turbulent structure and hence do not carry with them any of the constraints that other curves have in their application. As the model deals only with the absorption and has nothing to do with the properties of the emission sources, the FD05 curves can be applied to any given emission as they are not situation dependent.

In the NUV, using the same FD05 curve as for the FUV ($R_v = 4.5$) leads to an overestimation in the NUV SFRs compared to Hα-derived SFRs. There is agreement when $R_v = 6$ but this is inconsistent with other measured values, and with the value of R_v found to reconcile the FUV, Hα and [O II] measurements in our analysis. The fact that the NUV SFRs are overestimated more than the FUV SFRs in all MW obscuration curves and not in the Calzetti (2001) curve suggests that this effect is due to the 2200 Å feature being included in the extinction curve. The NUV being the only SFR indicator that otherwise does not agree with the other indicators lends weight to this argument as none of those wavelengths falls within the range of the 2200 Å feature. We show that the Hα and NUV-derived SFRs agree very well if the 2200 Å feature is eliminated in an FD05 curve with an R_v value of 4.5. This provides us with a consistent extinction correction curve for all the SFR indicators. The role of the 2200 Å feature will require further analysis in future work.

The use of the β parameter in estimating obscuration corrections for our sample of largely quiescent galaxies shows that intrinsic SFRs will be overestimated. Kong et al. (2004) attribute this to a secondary effect based on SFR histories.

6.2 SFR histories

We applied galaxy evolutionary synthesis models to the comparison between Hα and FUV-derived SFRs, and there was good agreement for all SFRs. The evolutionary paths were compared according to galaxy mass, characteristic decay time and IMF (assuming an exponentially decaying SFR).

We showed that by comparing the evolutionary paths for varying galaxy masses with observed data, we can identify a range of ages that the observed galaxies would fall into. This range was estimated to be between 200 and 500 Myr. There is a continuous variation in the ages making it difficult to identify any effects on the ages of galaxies due to mass. The IMFs we have tested show similar trends with a Baldry & Glazebrook (2003) IMF showing the best agreement with the observed data (Fig. 8a). This is particularly clear at the low SFR end with the Baldry & Glazebrook (2003) IMF following the observed SFR trend better than the other three IMFs. The Baldry & Glazebrook (2003) IMF has a faster evolution, where at any given SFR, the Baldry & Glazebrook (2003) evolutionary path has an age that is about 50Myr higher than the other tested IMFs.

The characteristic decay time was used to show how galaxies behave as they age: at low SFRs, a turn-off is expected away from the one-to-one line, towards the FUV SFR axis, as the Hα-derived SFRs decrease faster than FUV-derived SFRs. Our data do not extend to such low SFRs, but using PEGASE models we can recreate a predicted turn-off had our data extended to such low SFRs. The turn-off point is highly dependent on the characteristic decay time of SFRs with higher characterized decay times causing the turn off to occur later.

One of the proposed mechanisms for this behaviour is the Integrated Galaxy IMF (IGIMF) theory (Pflamm-Altenburg, Weidner & Kroupa 2007; Pflamm-Altenburg et al. 2009). Pflamm-Altenburg et al. (2007), Pflamm-Altenburg et al. (2009) constructed an integrated galactic IMF by combining all IMFs of all young star clusters. Using the IGIMF they predicted that the Hα luminosity of galaxies should decrease faster than UV luminosities at low SFRs as the Hα luminosity of star-forming dwarf galaxies decreases faster with decreasing SFR than the UV luminosity at low SFRs. This is clearly observed in the evolutionary paths in Figs 8(a) and (b). Pflamm-Altenburg et al. (2007, 2009) predict this turn-off to occur at around $10^{-2}\,M_\odot\,yr^{-1}$. As seen in Fig. 8(b) this turn-off can be replicated by a 90 Myr characteristic decay time which also agrees well with the observed data at higher SFRs. Even though our data do not extend far below an SFR of $10^{-2}\,M_\odot\,yr^{-1}$, the beginnings of such a trend can be observed in Figs 2(e), 7 and 8.

7 CONCLUSION

We find that an FD05 obscuration curve with an R_v value of 4.5 gives the best agreement across all SFR indicators provided that the 2200 Å feature is not included. These SFR distributions agree well with modelled evolutionary paths. We also show that the β parameter is not suitable for use with GALEX data.

Our main objective has been to obtain accurate dust extinction corrections for Hα and FUV and present a clear and concise formalism on how this is to be done based on various obscuration laws described in the literature. While the dust corrections were largely successful, we have identified key areas for further research, particularly in the significance of the 2200 Å in obscuration corrections. Analysing the effectiveness of extinction curves, particularly with IR data, will be of great significance for future work.

ACKNOWLEDGMENTS

DBW acknowledges the support provided by the Denison Scholarship from the School of Physics, University of Sydney. AMH

acknowledges support provided by the Australian Research Council through a QEII Fellowship (DP0557850).

REFERENCES

Adelberger K. L., Steidel C. C., 2000, ApJ, 544, 241
Afonso J., Hopkins A., Mobasher B., Almeida C., 2003, ApJ, 597, 269
Baldry I. K., Glazebrook K., 2003, ApJ, 593, 258
Baldry I. K., Glazebrook K., Brinkmann J., Ivezić Ž., Lupton R. H., Nichol R. C., Szalay A. S., 2004, ApJ, 600, 681
Baldry I. K. et al. 2010, MNRAS, 404, 86
Bell E. F., 2003, Revista Mexicana de Astronomía y Astrofisica, 17, 163
Bianchi L., Clayton G. C., Bohlin R. C., Hutchings J. B., Massey P., 1996, ApJ, 471, 203
Blanton M. R. et al., 2003, AJ, 125, 2348
Bouchet P., Lequeux J., Maurice E., Prévot L., Prévot-Burnhon M. L., 1985, A&A, 149, 330
Byun Y. I., Freeman K. C., Kylafis N. D., 1994, ApJ, 432, 114
Calzetti D., 1997a, in Waller W. H., Hollis J. E., Danks A. C., Fanelli M. C., eds, AIP Conf. Ser. Vol. 408, The Ultraviolet Universe at Low and High Redshift. Am. Inst. Phys., New York, p. 403
Calzetti D., 1997b, AJ, 113, 162
Calzetti D., 1999, Memoire della Societa Astronomica Italiana, 70, 715
Calzetti D., 2001, PASP, 113, 1449
Calzetti D., Kinney A. L., Storchi-Bergmann T., 1994, ApJ, 429, 582
Calzetti D., Armus L., Bohlin R. C., Kinney A. L., Koorneef J., Storchi-Bergmann T., 2000, AJ, 113, 162
Cardelli J. A., Clayton G. C., Mathis J. S., 1989, ApJ, 345, 245
Draine B. T. et al., 2007, ApJ, 663, 866
Driver S. P., Popescu C. C., Tuffs R. J., Liske J., Graham A. W., Allen P. D., De Propris R., 2007, MNRAS, 379, 1022
Driver S. P. et al., 2009, Astron. Geophysics, 50e, 12
Fanelli M. N., OConnell R. W., Thuan T. X., 1988, ApJ, 334, 665
Fioc M., Rocca-Volmerange B., 1997, A&A, 326, 950
Fischera J., Dopita M., 2005, ApJ, 619, 340 (FD05)
Fischera J., Dopita M. A., Sutherland R. S., 2003, ApJ, 599, L21
Fitzpatrick E. L., 1986, AJ, 92, 1068
Gilbank D. G., Baldry I. K., Balogh M. L., Glazebrook K., Bower R. G., 2010, MNRAS, 405, 2594
Hopkins A. M., Connolly A. J., Haarsma D. B., Cram L. E., 2001, AJ, 122, 288
Hopkins A. M. et al., 2003, ApJ, 599, 971
Keel W. C., 1993, in Cassinelli J. P., Churchwell E. B., eds, ASP Conf. Ser. Vol. 35, Massive Stars: Their Lives in the Interstellar Medium. Astron. Soc. Pac., San Francisco, p. 498
Kenney J. D. P., Carlstrom J. E., Young J. S., 1993, ApJ, 418, 687
Kennicutt R. C., Jr, 1983, ApJ, 272, 54
Kennicutt R. C., Jr, 1990, Astron. Space Sci. Libr., 161, 405
Kennicutt R. C., Jr, 1992a, ApJ, 338, 310
Kennicutt R. C., Jr, 1992b, ARA&A, 36, 189
Kewley L. J., 2006, MNRAS, 372, 961
Kewley L. J., Dopita M. A., Sutherland R. S., Heisler C. A., Trevena J., 2001, ApJ, 556, 221
Kong X., Charlot S., Brinchmann J., Fall S. M., 2004, MNRAS, 349, 769
Larson R. B., Tinsley B. M., 1978, ApJ, 219, L46
Lee J. C. et al., 2009, ApJ, 706, L599
Madau P., Pozzetti L., Dickinson M., 1998, ApJ, 498, 106
Mas-Hesse J. M., Kunth D., 1999, A&A, 349, 765
Meurer G. R., Heckman T. M., Calzetti D., 1999, ApJ, 521, 64
Nandy K., Thompson G. I., Jamar C., Monfils A., Wilson R., 1975, A&A, 44, 195
Norman C. A., Hasan H., Sellwood J. A., 1996, IAU Symp. 171, New Light on Galaxy Evolution. A&A, Heidelberg, p. 427
Osterbrock D. E., 1989, Astrophysics of Gaseous Nebulae and Active Galactic Nuclei. University Sci. Books, Mill Valley, CA
Pflamm-Altenburg J., Weidner C., Kroupa P., 2007, ApJ, 671, 1550
Pflamm-Altenburg J., Weidner C., Kroupa P., 2009, MNRAS, 395, 394
Pierini D., Gordon K. D., Witt A. N., Madsen G. J., 2004, ApJ, 617, 1022
Popescu C. C., Misiriotis A., Kylafis N. D., Tuffs R. J., Fischera J., 2000, A&A, 362, 138
Prévot M. L., Lequeux J., Prevot L., Maurice E., Rocca-Volmerange B., 1984, A&A, 132, 389
Robotham A. et al. 2010, PASA, 27, 76
Salim S. et al., 2007, ApJS, 173, 267
Salpeter E. E., 1955, ApJ, 121, 161S
Sanders D. B., Soifer B. T., Elias J. H., Madore B. F., Matthews K., Neugebauer G., Scoville N. Z., 1988, ApJ, 325, 74
Scalo J., 1998, in Gilmore G., Howell D., eds, ASP Conf. Ser. Vol. 142, The Stellar Initial Mass Function: 38th Herstmonceux Conference. Astron. Soc. Pac., San Francisco, p. 201
Seaton M. J., 1979, MNRAS, 187, 73P
Sharp R. et al., 2006, SPIE, 6269E, 14
Silva L., Granato G. L., Bressan A., Danese L., 1998, ApJ, 509, 103
Sullivan M., Treyer M. A., Ellis R. S., Bridges T. J., Milliard B., Donas J., 2000, MNRAS, 312, 442
Taylor E. N., Franx M., Glazebrook K., Brinchmann J., van der Wel A., van Dokkum P. G., 2010, ApJ, 722, 1
Tuffs R. J., Popescu C. C., Völk H. J., Kylafis N. D., Dopita M. A., 2004, A&A, 419, 821
van den Bergh S., 2007, AJ, 134, 1508
Wilkins S. M., Trentham N., Hopkins A. M., 2008a, MNRAS, 385, 687
Wilkins S. M., Hopkins A. M., Trentham N., Tojeiro R., 2008b, MNRAS, 391, 363
Witt A. N., Thronson J., H. A., Capuano J. M., Jr, 1992, ApJ, 393, 611
Xilouris E. M., Kylafis N. D., Papamastorakis J., Paleologou E. V., Haerendel G., 1997, A&A, 325, 135
Xilouris E. M., Alton P. B., Davies J. I., 1998, A&A, 331, 894
Xilouris E. M., Byun Y. I., Kylafis N. D., Paleologou E. V., Papamastorakis J., 1999, A&A, 344, 868

This paper has been typeset from a TEX/LATEX file prepared by the author.